Energy Advances

Accepted Manuscript

This article can be cited before page numbers have been issued, to do this please use: M. masood, M. Aamir, M. E. Khan, M. Sher, K. khan, H. Zahid Shafi, Md. Akhtaruzzaman, H. Almohamadi and Md. Shahiduzzaman, *Energy Adv.*, 2024, DOI: 10.1039/D4YA00327F.

ROYAL SOCIETY OF CHEMISTRY

rsc.li/energy-advances

View Article Online
DOI: 10.1039/D4YA00327F

- No software or code have been included and no new data were generated or analysed as part of this study.

View Article Online
DOI: 10.1039/D4YA00327F

ARTICLE

Unrevealing the Potential of Multicomponent Metal ion Incorporation and Sulfide Modification in Cobalt Oxide for Efficient Water Oxidation

Received 00th January 20xx,
Accepted 00th January 20xx

DOI: 10.1039/x0xx00000x

Muzzayab Masood[a], Muhammad Aamir[a]*, Muhammad Ejaz Khan[b], Muhammad Sher[c], Khush Bakhat Akram,[c] Hafiz Zahid Shafi,[d] Hamad Almohamadi,[e] Md. Akhtaruzzaman,*[f] Md. Shahiduzzaman,[g]

The designing and development of highly efficient electrocatalysts from transition metals have shown a great potential for substituting precious meta-based electrocatalysts in water splitting processes. Cobalt oxide is one of the promising materials for oxygen evolution reactions (OER). Modifying the metal oxide by the incorporation of metal ions and substituting sulfides are effective but challenging strategies for efficient OER activities. In the present work, we report the synthesis of CdCoO and CdCoS electrocatalysts deposited on the surface of nickel foam. These electrocatalysts and their composites CdCoO@CuCoO and CdCoS@CuCoS deliver high catalytic activity for oxygen evolution reaction. The as-synthesized electrocatalysts were characterized by pXRD, FTIR, Raman, XPS, SEM techniques. The CdCoS showed a lower OER overpotential of 199 mV at the current density of 10 $mAcm^{-2}$ and 522 mV at 60 $mAcm^{-2}$). The incorporation of Cd^{2+} ions in cobalt oxides optimized the electronic states around the Co-active sites causing improved catalytic activities by showing a lower overpotential compared to variously reported cobalt oxides(oxyhydroxides). This work emphasizes the effect of metal ion incorporation and sulfide modification on the OER activity of cobalt oxide for water splitting and provides a multi-component engineering strategy for designing efficient electrocatalysts.

Introduction

The development of efficient and cost-effective electrocatalysts for the oxygen evolution reaction (OER) remains a serious challenge for realizing the full potential of electrochemical water splitting as a clean and sustainable energy source.[1-3] This technology holds immense promise for generating hydrogen fuel, a clean-burning fuel with minimal environmental impact.[4-7] Transition metal oxides, phosphides, and sulfides have emerged as promising OER electrocatalysts owing to their inherent abundance, good stability, and tunable physicochemical properties.[8, 9] The electrocatalytic activity of transition metal oxides can be tuned by the intentional incorporation of metal ions and the substitution of sulfur in the metal oxides, which collectively enhanced their OER activity.[10, 11] Thus, the sulfur incorporation in the metal oxides particularly in the cobalt oxide produces the high spin state of Co^{3+} ions. This high spin state has a higher electron population in the *eg*-orbitals of Co^{3+}, improving the OER activity of the cobalt oxide and its derivatives.[12]

The metal sulfides have an enormous potential for development, however, it shows lower conductivity and scarcity of active sites are major challenges for their widespread applications.[13] These challenges were addressed by various strategies such as the combination of metal sulfides with oxides to create heterojunctions that subsequently improve the conductivity.[11, 14] Likewise, tuning the electronic properties of the metal oxides by introducing the sulfur by partial substitution results in lowering the covalency of the M-O bond through an inductive effect.[15] The sulfur withdraws the electron density in the M-O-S bond and lowers the energy of antibonding orbitals, which promotes the formation of a high spin metal system with enhanced OER activities. [16, 17]

Likewise, the substitution of metal ions in metal sulfide or metal incorporation in the metal sulfides optimized the local electronic structure of the active sites available for OER activities. The metal ions, such as those with n-type or p-type, incorporations in the cobalt oxide and sulfides could be worth full to explore. For instance, Cd incorporation in the cobalt oxide promotes electron transfer at the cobalt active sites. Moreover, the larger Cd^{2+} ion produces distortion in the cobalt oxide lattice causing the exposure of cobalt sites for OER activities.[18]

[a] Department of Chemistry, Mirpur University of Science and Technology (MUST), Mirpur-10250 (AJK), Pakistan. Email: aamirorg@gmail.com
[b] 2 Department of Computer Engineering, National University of Technology, Islamabad 44000, Pakistan
[c] 3Department of Chemistry, Allama Iqbal Open University, H-8, Islamabad, Pakistan
[d] Materials Division, National Institute of Lasers & Optronics College (NILOP-C), Pakistan Institute of Engineering & Applied Science (PIEAS), P.O. Nilore 45650, Islamabad, Pakistan
[e] Department of Chemical Engineering, Faculty of Engineering, Islamic University of Madinah, Madinah, Abo Bakr Al Siddiq, Al Jamiah, Madinah 42351, Saudi Arabia
[f] The Department of Chemistry, Faculty of Science, The Islamic University of Madinah, Madinah, Abo Bakr Al Siddiq, Al Jamiah, Madinah 42351, Saudi Arabia Email: akhtar.brces@gmail.com
[g] Nanomaterials Research Institute, Kanazawa University, Kakuma, Kanazawa 920-1192, Japan
† Footnotes relating to the title and/or authors should appear here.
Electronic Supplementary Information (ESI) available: [details of any supplementary information available should be included here]. See DOI: 10.1039/x0xx00000x

View Article Online
DOI: 10.1039/D4YA00377F

Whereas, the ionic radii of Cu^{2+} ions are comparable to Co^{3+} ions. It has also been reported that Cu-incorporated cobalt oxides with some optimum copper concentration have improved the OER activity of the cobalt oxides for OER.[19] Moreover, the electronegativity of the Cd^{2+} ions and Cu^{2+} is less than Co^{3+} ions, the CdO are n-type and CuO are p-type materials which affect the electronic properties of the active sites.[20] Recently, the development of multi-elemental materials also known as high entropy materials having multiple elements in solid solutions and composites have been explored and have shown excellent OER performances.[21-23]

In this work, we successfully synthesized the Cd-incorporated cobalt oxide and the multi-component composite of CdCoO with CuCoO. The sulfurized analogs were also synthesized through a deliberate design using sulfur precursors. The characterizations were performed by using pXRD, XPS, FTIR, Raman, and SEM techniques to analyze the as-synthesized materials. The electrochemcial results showed that the OER potential is lower in Cd incorporated cobalt oxide but the over-potential was increased in composites. The sulfide analog of the aforementioned electrocatalysts has shown lower over-potential than oxides. The experimental results confirmed the influence of metal ion substitution in the metal oxides and sulfides on the electronic properties around the active sites and the effect of sulfide on the OER activity of the electrocatalysts. These findings will provide the fundamental understanding to design the new materials to improve the OER activities.

Experimental

Chemicals

The commercially available analytical grade chemicals were used without further purification. These included cadmium sulfate hydrate ($CdSO_4 \cdot 8/3H_2O$), cobalt(II) sulfate heptahydrate ($CoSO_4 \cdot 7H_2O$), copper(II) sulfate pentahydrate ($CuSO_4 \cdot 5H_2O$), thiourea (CH_4N_2S), ammonium dihydrogen phosphate ($NH_4H_2PO_4$), polyvinylpyrrolidone (PVP, K-30, MW 40,000), 2-methylimidazole ($C_4H_6N_2$), glycerol, isopropyl alcohol (IPA), N,N-dimethylformamide (DMF), ethanol, and deionized water. All chemicals were purchased from Sigma Aldrich.

Synthesis of electrocatalysts CdCoO and CdCoS

A solvothermal method was employed for the synthesis of CdCoO. Briefly, 0.125 g of $CdSO_4$ and 0.25 g of $CoSO_4$ were dissolved in 40 mL of isopropyl alcohol under magnetic stirring for 30 minutes. Subsequently, 8 mL of glycerol was added, and the solution was stirred for another hour to obtain a light pink homogeneous mixture. This mixture was then heated at 180 °C for 6 hours in a sealed container. The resulting CdCo-glycolate precursor was cooled down, collected by centrifugation, and washed thoroughly with ethanol and deionized water. Finally, the dried CdCo-glycolate was calcined at 350 °C for 2 hours to obtain CdCoO nanoparticles. For the synthesis of CdCoS, 0.2 g of thiourea was added to the reaction mixture alongside $CdSO_4$ and $CoSO_4$ using the same procedures described for CdCoO.

Synthesis of CdCoO@CuCoO and CdCoS@CuCoS

The Cd–Co–O@Cu–Co–MOF composite was synthesized via a two-step method. Firstly, 0.175 mg of PVP was dissolved in 10 mL of ethanol and stirred with 0.35 mg of pre-synthesized Cd–Co–O for 12 hours. Subsequently, 10 mL each of deionized water and DMF were added along with 2 g of PVP, 0.25 mg of $CoSO_4 \cdot 6H_2O$, 0.75 mg of 2-methylimidazole, and 1.25 mg of $CuSO_4 \cdot H_2O$. The mixture was stirred for 30 minutes to achieve homogeneity and then heated at 150 °C for 10 hours in a sealed container. The obtained product was cooled down, centrifuged at 6000 rpm for 15 minutes, washed repeatedly with appropriate solvents, and dried to obtain the Cd–Co–O@Cu–Co–MOF precursor. The synthesis of CdCoS@CuCo-MOF followed the same procedure, utilizing CdCoS instead of CdCoO in the initial step. CdCoO@CuCoO and CdCoS@CuCoS nanocomposites (NCs) were fabricated by thermal decomposition of the corresponding MOF precursors (M = Co or S). The calcination process was carried out at 450 °C for 2 hours with a heating rate of 1 °C min^{-1} in air. Scheme 1 shows the steps involved in the synthesis of CdCoS and CdCoS@CuCoS-CNs composite.

Structural Characterizations

The pXRD diffraction pattern was determined by using the Bruker-D8 discover system, Germany under Cu Kα X-ray irradiation with λ = 1.5406 Å. Scanning electron microscopy (SEM) and energy dispersive X-ray (EDX) analysis were performed to obtain images and elemental composition using the FESEM NOVA MIRA3XMM instrument. Fourier transform infrared spectroscopy (FT-IR) was performed to identify functional groups using SHIMADZU IRAffinity-1S at room temperature. The XPS was measured by a Kratos Axis Ultra DLD, Kratos Analytical, Japan based UHV spectrometer equipped with an Al Kα X-ray irradiation source (1486.6 eV).

Electrochemical OER measurements

The electrochemical measurements were performed by using an electrochemical workstation (Gamry Reference 3000) in three electrode setup with 15 mL aqueous KOH as an electrolyte, as-prepared samples on nickel foam as the working electrode, Pt as the counter electrode, and Ag/AgCl as reference electrode. Electrochemical techniques such as cyclic voltammetry (CV), linear sweep voltammetry (LSV), and electrochemical impedance spectroscopy (EIS) were employed to evaluate the performance of electrocatalysts for OER activities.

Linear sweep voltammetry (LSV) Measurements

The scan rate was set at 5 mVs^{-1} to get the precise overpotential. The conversion between the potentials versus Ag/AgCl and RHE was calculated by using Nernst equation (1) as follows.

$$E_{RHE} = E_{Ag/AgCl} + (0.1976 + 0.059\,pH)V \quad (1)$$

The overpotential of the electrocatalyst was determined by equation (2).

$$Overpotential = E_{RHE} - 1.23\,V \quad (2)$$

Tafel plots

View Article Online
DOI: 10.1039/D4YA00327F

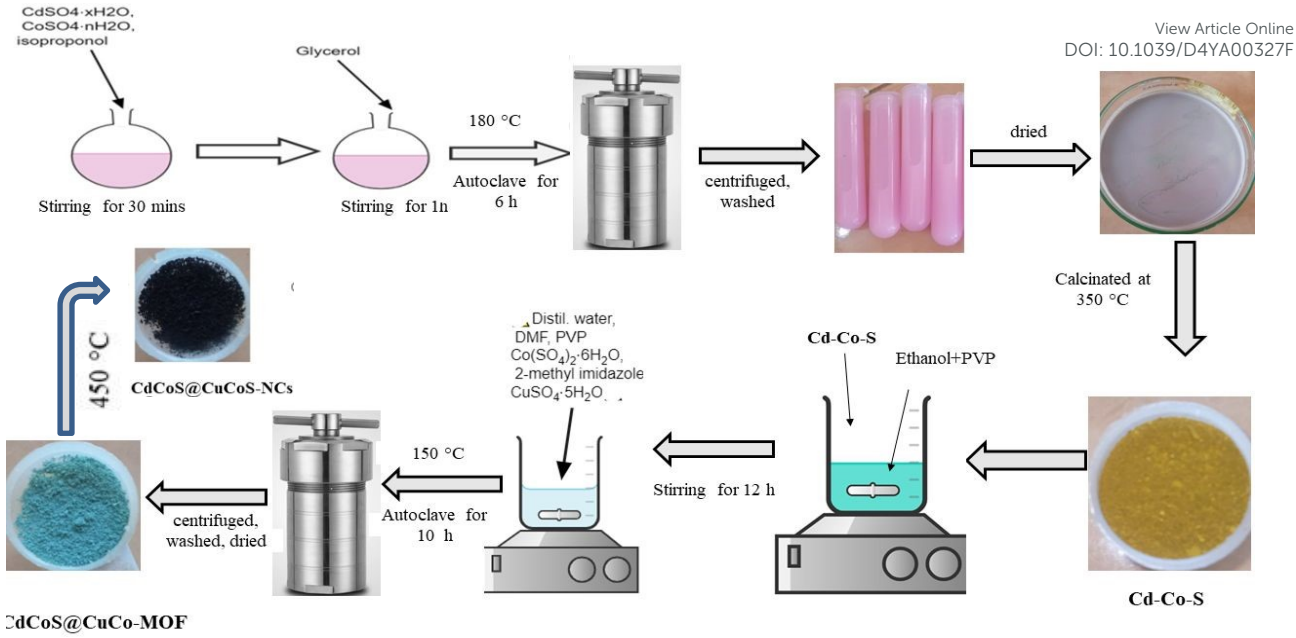

Scheme 1. Schematic illustration for the synthesis of CdCoS and its composite CdCoS@CuCoS-NCs.

The polarization curves obtained from the LSV measurements were plotted as overpotential versus the log current. The Tafel slope was obtained by taking the slope of the fitted linear portion of the Tafel plot according to the following equation (3).

$$\eta = b\ log[J] + a \quad (3)$$

Where **η** is the overpotential in V, J is the current density in $mAcm^{-2}$ and b is the Tafel slope in $mVdec^{-1}$. The double-layer capacitance (Cdl) was determined by using CV data obtained at different scan rates. The electrochemical surface area (ECSA) was calculated using equation (4).

$$ECSA = \frac{C_{dl}}{C_s} \quad (4)$$

Where Cs is the specific capacitance of materials.

***iR* corrections**

The solution resistance was determined by the impedance spectroscopy. The potential was corrected by 100% of solution resistance according to equation (5).

$$E_{iR\ corrected} = E - iR \quad (5)$$

Results and Discussion

FTIR spectra of the as-synthesized CdCoO, CdCoO@CuCoO/C-NC, CdCoS, and CdCoS@CuCoS/C-NC are presented in Figure 1a. The stretching vibrational bands at 1635 cm^{-1} and 3266 cm^{-1} are credited to the -OH group present on the surface of CdCoO and its derivatives.[24] The presence of H_2O and CO_2 is indicated by the symmetric and asymmetric stretching of C-O vibrations observed at 1000-1500 cm^{-1}.[25] A band located at 2358 cm^{-1} corresponds to the stretching vibrations of C-H bonds.[26] Sharp bands at 592 cm^{-1} and 675 cm^{-1} indicate the presence of spinel structure vibrations of M-O bond vibrations in tetrahedral and octahedral fields.[27,28] In CdCoO@CuCoO/C-NC, the M-O vibrational bands become weaker and broader due to the formation of M-O, M-N, and M-C bonds due to the metal oxides and oxygen and nitrogen functionalized carbons.[29] Likewise, a band at 1618 cm^{-1} indicates the presence of C=C linkage in

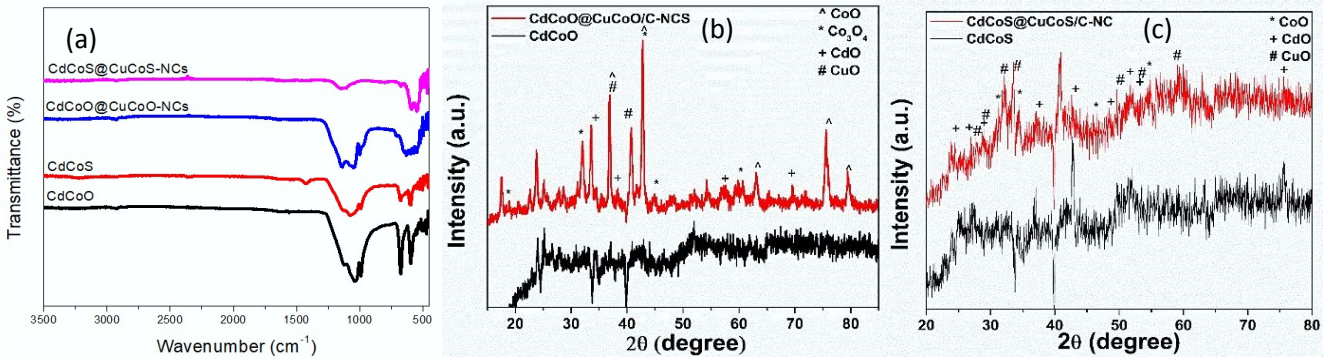

Figure 1. (a) FTIR spectra of CdCoO, CdCoS, CdCoO@CuCoO-NCs and CdCoS@CuCoS-NCs. pXRD patterns of (b) CdCoO, CdCoO@CuCoO-NCs (c) CdCoS, and CdCoS@CuCoS-NCs.

CdCoO@CuCoO/C-NC.[25] Symmetric stretching of C-O appears at 1024 cm^{-1}. In CdCoS, the vibrational bands at 592 cm^{-1} and 671 cm^{-1} belong to Co-S and Cd-S, respectively. [26] Similar to oxide-based samples, the weak vibrational band of M-S in CdCoS@CuCoS/C-NC has also become further broader and weaker.

The crystal structure of the as-synthesized samples was determined by X-ray diffraction (XRD) analysis. Figure 1b shows the XRD patterns of CdCoO and CdCoO@CuCoO/C-NCs. The diffraction peaks at 2θ degrees of 18.9, 32, 36.9, 42.7, 44.9, and 60.77 degrees are indexed to (111), (220), (311), (222), (400), (422), (511), and (440) planes of Co_3O_4 (JCPD Card: 75-2480).[30] According to JCPD file No. 01-074-2391, the presence of CoO is confirmed by the peaks diffracted at 2θ degrees of 36.9, 42.7, 63.05, 75.7, and 79.2 are indexed to planes (111), (200), (220),

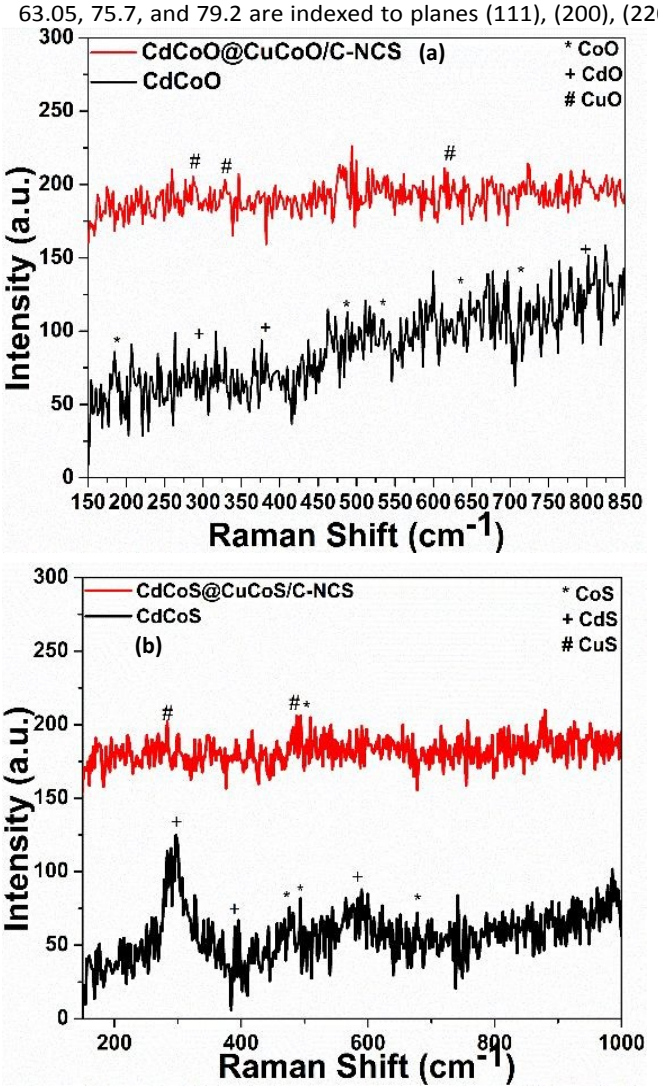

Figure 2. Raman spectra of **(a)** CdCoO and CdCoO@CuCoO/C-NCs **(b)** CdCoS and CdCoS@CuCoS/C-NCs

(311), and (222). [31] The presence of Cd-O was confirmed by the appearance of diffraction peaks (111), (200), (220), (311), and (222) at degree angles 33.6, 38.2, 57.1, and 69.5 (JCPD card no 75-0592).[32] Two diffraction peaks (200) and (111) at 36.9 and 40.8 degrees appeared from the incorporation of CuO (JCPD card 45-0937) in CdCoO@CuCoO/C-NCS.[33] Similarly, in CdCoS and CdCoS@CuCoS/C-NCs, the diffraction peaks at degree angles of 31.2, 34.5, 46.6, and 54.7 are consistent with JCPD card # 19-0366, which correspond to (204), (220), (306), and (330) planes of CoS (figure 1c).[34] The diffraction peaks of CdS appear at 2θ degrees of 23.9, 27, 28.5, 37.09, 42.8, 51.9, and 53.6 belong to the planes (100), (002), (101), (102), (110),(103), (200),(112), and (201) respectively.[35] The diffraction peaks observed at degree angles of 27.8, 29.1, 32.1, 33.4, 49.9, 53.5, and 59 were found to have characteristics of CuS and assigned to indices (1010), (102), (103), (006), (110), (108), and (116), respectively (JCPD No. 01-079-2321).[36]

The vibrations of metal-oxygen bonds, nearby surface imperfections, and the coordinating environment are all investigated using Raman spectroscopy. Raman spectra of prepared oxide nanocomposites are shown in Figure 2a. All the characteristic vibration peaks of CdCoO can be seen in Raman spectra. Vibrational peaks at 184.8 cm^{-1}, 487.92 cm^{-1}, 524.6 cm^{-1}, 636.01 cm^{-1}, and 713 cm^{-1} are assigned to asymmetric and bending vibrations of Co_2O_3.[37] CdO exhibits raman modes at 281 cm^{-1}, 376 cm^{-1}, 599.7 cm^{-1}, and 801 cm^{-1}.[38] In CdCoO@CuCoO/C-NCs, peaks at 287.18 cm^{-1}, 328 cm^{-1}, and 615 cm^{-1} are assigned to the vibrations of Cu-O.[39] In the case of CdCoS, vibrations at 477.6 cm^{-1}, 494 cm^{-1}, and 677.3 cm^{-1} and peaks at 298.9 cm^{-1}, 392.2 cm^{-1}, and 586.7 cm^{-1} are assigned to the Raman modes of CoS and CdS, respectively (figure 2b).[35,40] Likewise, in CdCoS@CuCoS/C-NCS, vibrational modes for CuS at 285.1 cm^{-1} and 485.2 cm^{-1} are the characteristics peaks for Cu-S bond(figure 2b).[41]

The X-ray photoelectron spectroscopy was recorded on the surface of as-synthesized materials to examine their valence shell states. The XPS survey spectrum of CdCoO, and CdCoO@CuCoO/C-NCs (CdCoO@CuCoO) is shown in figure 3a. The presence of Cd, Co, C, and O at the surface of synthesized materials can be observed in the survey spectra of CdCoO. The only difference in the XPS survey spectra of CdCoO@CuCoO and CdCoO is the presence of Cu-related peaks, indicating the successful formation of required materials. Figure 3b shows the comparative survey XPS spectrum of CdCoS and CdCoS@CuCoS/C-NCs (CdCoS@CuCoS). The presence of S2p peaks in the survey spectrum shows the formation of respective sulfides. Figure 3c shows the major peaks at 406 eV and 412 eV correspond to Cd $3d^{3/2}$ and Cd $3d^{5/2}$, respectively, confirming the presence of Cd^{+2}.[42,43] Whereas, the deconvoluted spectra of Co2p with spin-orbit bimodal pairs show the peaks of Co $2p^{1/2}$ and Co $2p^{3/2}$ which appear at 798.6 eV and 783. 6 eV, respectively with the satellite peaks at 804 and 786 eV, confirming the presence of CoO (figure 3c). [44, 45] The oxidation state of the cobalt can not be determined purely on main oxidation peaks.[46] The satellite peak intensity and their binding energy positions are to identify the Co valance state.[47] Cobalt shows 2+ and 3+ ionic states in which Co^{2+} displays the two satellite peaks due to the crystal field splitting in the tetrahedral crystal field environment. Therefore, it is obvious from the spectrum that the cobalt present in mixed valance states in the as-synthesized materials.[46, 48]

Figure 3d displays the deconvoluted spectra of Cu2p into cu $2p^{3/2}$ and cu $2p^{1/2}$ at 935.1 eV and 955.1 eV, respectively. The

energy difference between the two peaks is 20 eV which corresponds to the previous CuO spectra. [49] Two satellite peaks at 943 eV and 962.6 eV with the main peaks also confirm the synthesis of CuO. [50, 51] The core level spectrum of O1s is illustrated in Figure 3(d). A distinct peak at 532 eV is attributed to the O^{-2}.[52] Similarly, spectral peaks for C1s appear at 292.1, 287.5, and 284.9 eV are attributed to the presence of C-O and C-C linkages due to the oxidation of imidazole to form carbons (figure 3e).[53] Similarly, in CdCoS@CdCuS, peaks for S^{-2} were observed at 168 eV and 170 eV for $S2p^{3/2}$ and $S2p^{1/2}$, respectively (Figure 3g). [54, 55]A peak at 171.2 eV corresponds to the presence of metal-sulfur linkage. [56] The presence of S2p and O1s characteristic peaks in the sulfide-based samples indicates the formation of partial sulfide and oxide-based systems (figure 3h).

Scanning electron microscopy (SEM) was used to explore the morphology of the as-synthesized materials as shown in Figure 4. Figure 4a shows that the CdCoO has flake-like aggregated microstructures. The CdCoO@CuCoO composite shows flower-like morphologies due to the presence of carbon materials (figure 4b). Whereas, CdCoS exhibited smaller fused spherical morphologies due to the agglomeration as displayed in Figure 4c. In comparison to the CdCoO, the CdCoS has smaller particles. Like CdCoO@CuCoO, the CdCoS@CuCoS composites have similar kinds of flake-like structures due to the carbon materials (figure 4d).

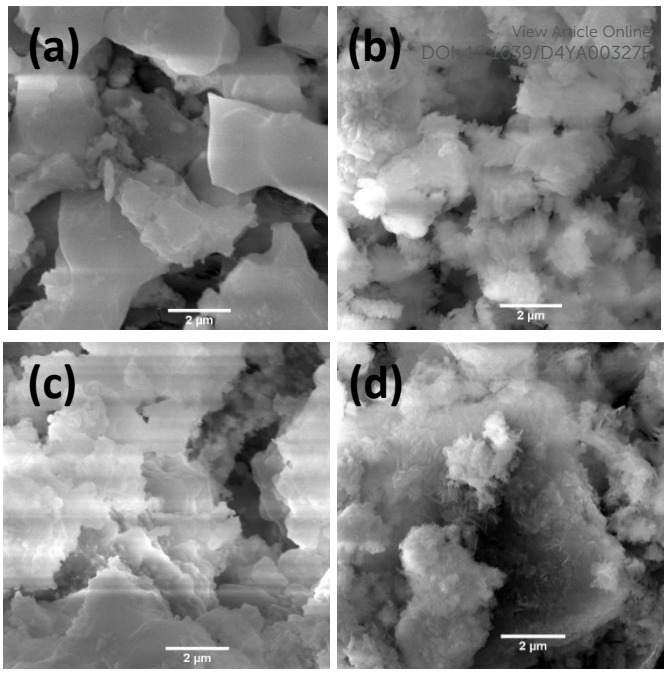

Figure 4. SEM images of as-synthesized (a) CdCoO, (b) CdCoO@CuCoO, (c) CdCoS, and (d) CdCoS@CuCoS.

Electrochemical OER Activity

The as-synthesized materials have shown typical cyclic voltammetry (CV) behavior in 1.0 M KOH as shown in Figure 5a-d. The oxidation peak between 1.42-1.66 V (vs. RHE) corresponds to the Co^{2+}/Co^{3+} redox couple which is an active electrocatalyst for OER activity. The plot between the anodic peak current and the square root of the scan rate exhibits a linear relationship (figure 5e). The slope values for CdCoS, CdCoS@CuCoS, CdCoO, and CdCoO@CuCoO are 33.1784, 27.6949, 16.8722, and 17.6006 respectively. The highest slope value was observed for CdCoS indicating the enhanced diffusion properties of OH^-. Therefore, more electroactive supplies such as Co-SOOH can be formed on the surface of CdCoS. Likewise, the CV profiles were also used to determine the double-layer capacitance (Cdl) of as-synthesized catalysts as presented in Figure 5f.

The average Cdl of CdCoS, CdCuS@CuCoS, CdCoO, and CdCoO@CuCoO were found to be 0.34 $mFcm^{-2}$, 0.20 $mFcm^{-2}$, 0.069 $mFcm^{-2}$ and 0.068 $mFcm^{-2}$ respectively (Table 1). The larger Cdl value of CdCoS also suggests the more active sites for

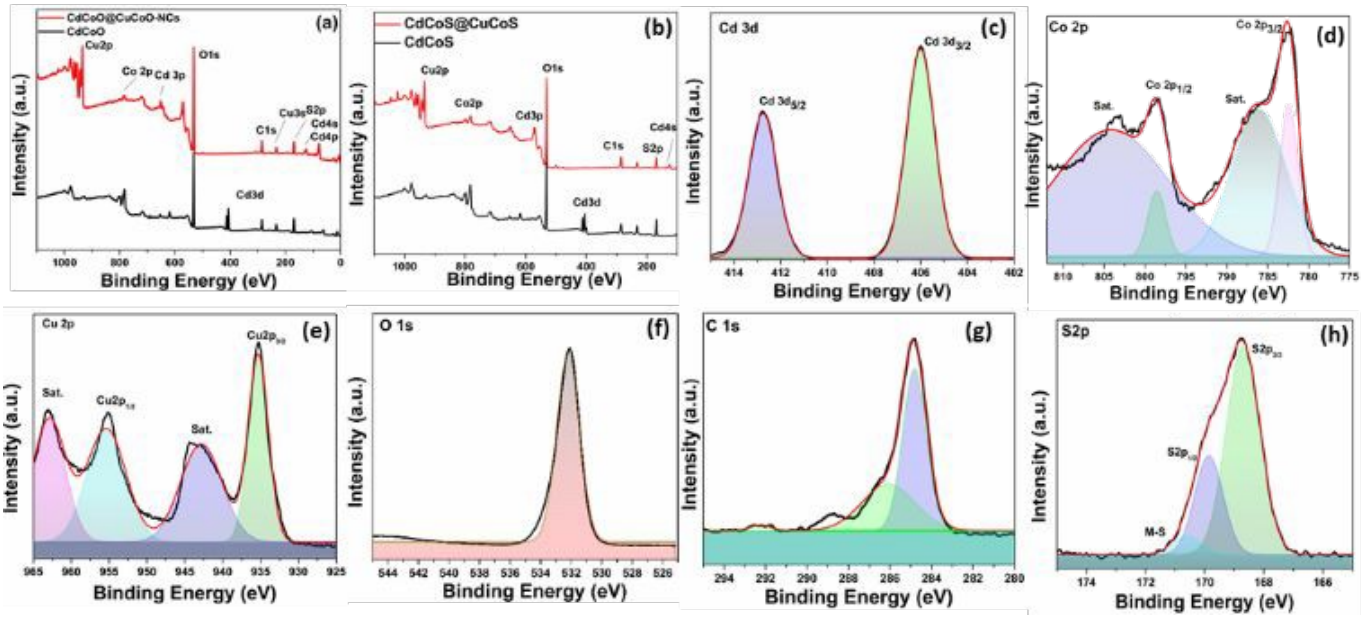

Figure 3. XPS survey spectra of (a) CdCoO, CdCoO@CuCoO/CNs, and (b) CdCoS and CdCoS@CuCO@/CNs. XPS is the deconvoluted spectra of (c) Cd, (d) Co, (e)Cu, (f)O,(g) C, and (h) S in the as-synthesized samples.

View Article Online
DOI: 10.1039/D4YA00327F

the OER activity. The Cdl results support the finding of the anodic peak current and the square root of the scan rate plot. The ECSA is another parameter to correlate the catalytic efficiency of the materials and was calculated by using average Cdl values as presented in Table 1.

Table 1. Experimental parameters of as-synthesized electrocatalyst materials

Catalysts	Average Cdl ($mFcm^{-2}$)	ECSA (cm^{-2})	Rct (Ω)
CdCoS	0.34	15.22	3.2
CdCoS@CuCoS	0.20	8.95	8
CdCoO	0.068	3.045	10.78
CdCoO@CuCoO	0.069	3.09	23.2

The CdCoS shows the ECSA value of 15.22 cm^{-2}, whereas, ESCA for CdCuS@CuCoS, CdCoO, and CdCoO@CuCoO are 8.95, 3.045, and 3.09 cm^{-2} respectively (table 1). The greater ESCA value for the CdCoS shows that it offers a large surface area and active sites for the intrinsic electrocatalytic activity of the catalyst compared to the other as-synthesized materials. Based on these results, it can be determined that the CdCoS and CdCoO can show more electrocatalytic performance than the composites since the composites are of large-sized particles with reduced surface area, moreover, the surface of the catalyst is covered by the amorphous carbon which blocks the active sites.

LSV was performed using a standard three-electrode system in 1.0 M KOH alkaline media at the potential window of 1.2-2.3 V (*vs*. RHE) to explore the electrochemical OER performance of the as-synthesized catalysts. As shown in Figure 6a, the onset potential for CdCoS, CdCuS@CuCoS, CdCoO, and CdCoO@CuCoO were observed at 1.42 V, 1.435V, 1.438 V and 1.446 V (*vs*. RHE), respectively.

Whereas values of over-potential at 10 $mAcm^{-2}$ are 199 mV, 205 mV, 208 mV, and 215 mV for CdCoS, CdCuS@CuCoS, CdCoO and CdCoO@CuCoO respectively. It can be observed that the CdCoS shows lower over-potential than all other as-synthesized catalysts. However, these overpotential values at 10 $mAcm^{-2}$ do not truly represent the overpotential for the OER. There is a contribution from the oxidation peak current of materials in the same potential range. Thus, we also measured the overpotential at 60 $mAcm^{-2}$ to eliminate the oxidation peak current factor. At 60 $mAcm^{-2}$, there was no involvement of oxidation peaks of the as-synthesized catalysts. The overpotential values show the same trend as observed at 10 $mAcm^{-2}$, however, the value of overpotential was high as expected. The overpotential values for CdCoS, CdCuS@CuCoS, CdCoO, and CdCoO@CuCoO are 522 mV, 588 mV, 543 mV, and 616 mV at 60 $mAcm^{-2}$, respectively. It can be observed that the CdCoS and CdCoO have superior performance compared to their respective composites CdCoS@CuCoS and CdCoO@CuCoO. These results indicate the poor charge transfer between the heterostructures, increased particle size after the formation of composite, and blockage of active sites by the carbon are the major contributors.

Likewise, we have calculated the TOF value of as-synthesized electrocatalysts to determine the intrinsic activity of catalysts, by assuming that the Co^{2+} is the only active sites and is oxidized just before the onset of OER. The TOF value were calculated at 10 $mAcm^{-2}$ and 60 $mAcm^{-2}$. CdCoS shows the 0.673 s^{-1} (10

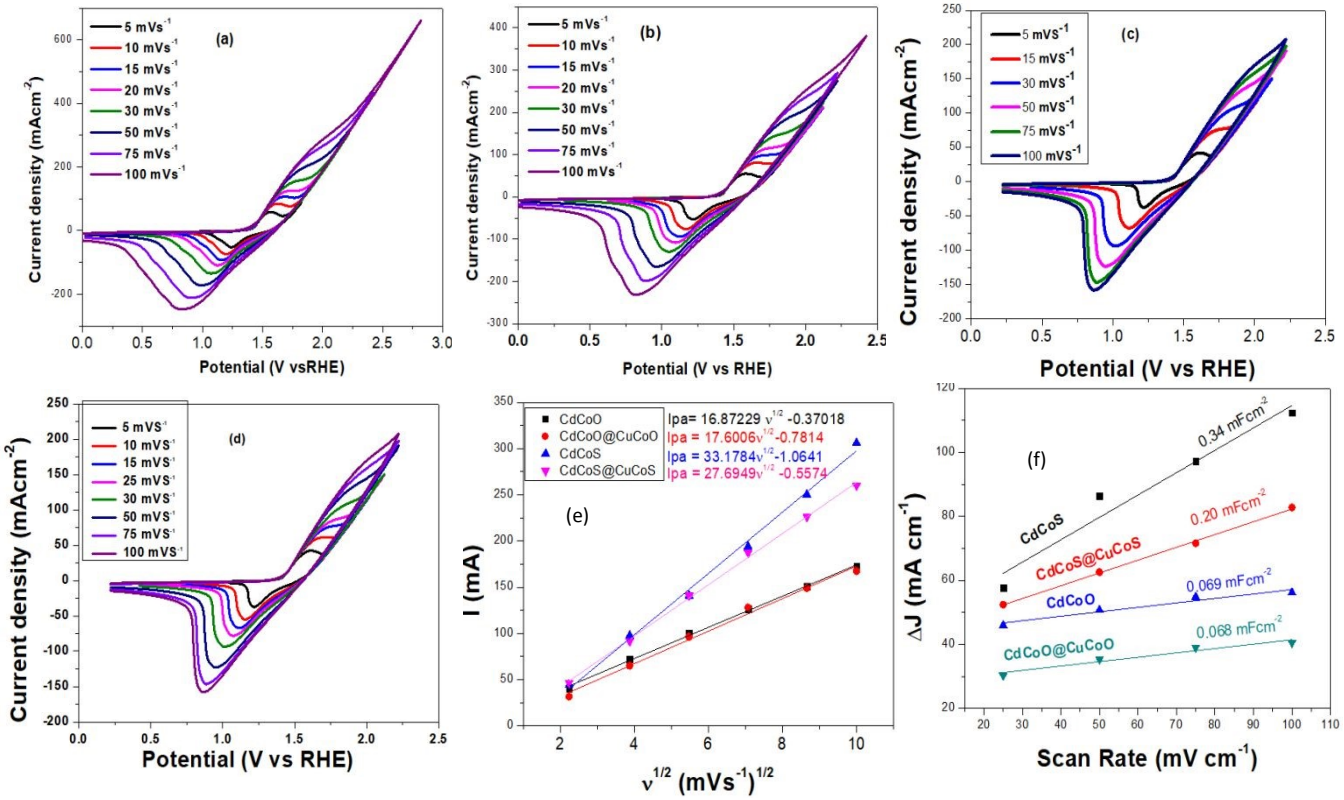

Figure 5. Cyclic voltammograms (CV) of the catalysts (a) CdCoS, (b) CdCoS@CuCoS, (c) CdCoO and CdCoO@CuCoO. The plot between the anodic peak current (Ipa) of cyclic voltammograms in 1.0 M KOH and the square root of the scan rates ($v^{1/2}$) for all as-synthesized catalysts.

View Article Online
DOI: 10.1039/D4YA00727F

mAcm^{-2}) and 4.04 s^{-1} (60 mAcm^{-2}) while, TOF values of 1.04 s^{-1} (10 mAcm^{-2}) and 6.26 s^{-1} (60 mAcm^{-2}) observed for CdCoO. On the other hand, for CdCuS@CuCoS, the TOF values were 1.1 s^{-1} (10 mAcm^{-2}) and 6.59 s^{-1} (60 mAcm^{-2}) and for CdCoO@CuCoO, 1.32 s^{-1} (10 mAcm^{-2}) and 7.93 s^{-1} (60 mAcm^{-2}) TOF values were observed.

Table 2. Overpotential calculated from uncorrected *iR* LSVs and Tafel slope results to evaluate the electrocatalytic activity of as-synthesized materials.

Catalyst	Over-potential (mV)		Tafel Slope (mVdec^{-1})
	At 10 mAcm^{-2}	At 60 mAcm^{-2}	
CdCoS	199	522	63.45
CdCoO	208	543	81.98
CdCoS@CuCoS	205	588	69.91
CdCoO@CuCoO	215	616	83.05

As the electrocatalysis was performed in the solution phase, therefore, solution resistance play a key role in the electrocatalysis. To determine the solution resistance, electrochemical impedance spectroscopy (EIS) was performed and the results are presented in Figure 6b. EIS was performed in 1.0 M KOH solution, at open circuit potential. Solution resistance of 1.27, 2.14, 2.94, and 3.41 Ω have been observed for CdCoS, CdCuS@CuCoS, CdCoO, and CdCoO@CuCoO catalysts, respectively. The Rct values for CdCoS, CdCuS@CuCoS, CdCoO, and CdCoO@CuCoO are 3.2, 8, 10.78, and 23.2 Ω respectively. The lowest Rct value was observed for CdCoS indicating the faster electron transport compared to other electrocatalysts.

Kinetics is another parameter to determine the performance of the electrocatalyst. Figure 6c shows the Tafel plot for CdCoS, CdCuS@CuCoS, CdCoO, and CdCoO@CuCoO are 63.45 mV/dec, 69.91 mV/dec, 81.98 mV/dec, and 83.05 mV/dec respectively. CdCoS shows the lowest Tafel slope value indicating the fast kinetics compared to all other samples. Likewise, in comparison, the CdCoS has a lower Tafel slope value compared to the CdCoS@cuCoS whereas, the CdCoO is lower than the corresponding composite (table 2). The results are in coherence with the LSV results. The stability of the prepared catalyst was determined at the constant voltage of 0.6 V and the current was measured for 7 hours as shown in Figure 6d. A slight decrease in current density was observed after a few hours, but overall the catalyst exhibited good stability for 7 hours.

Activity Enhancements in the As-synthesized Electrocatalysts

Zheng *et al*.[11] compared the OER activity of the CuCoO and CuCoS by partially substituting the oxides with sulfides. It was revealed that the charge density of the Co-active sites was increased due to the removal of highly electronegative oxygen atoms, thus a low valence state of the central metal was observed. The increase in the electron density on the Co^{3+} state results in the change of electron-filled configuration $t2g^6\ eg^1$ in the crystal field, which becomes close to the Co^{2+} ions. According to the *eg*-orbital theory, if the electron in the *eg* orbital is greater than 1, the adsorption capacity for OER intermediates becomes weak, and appropriate adsorption

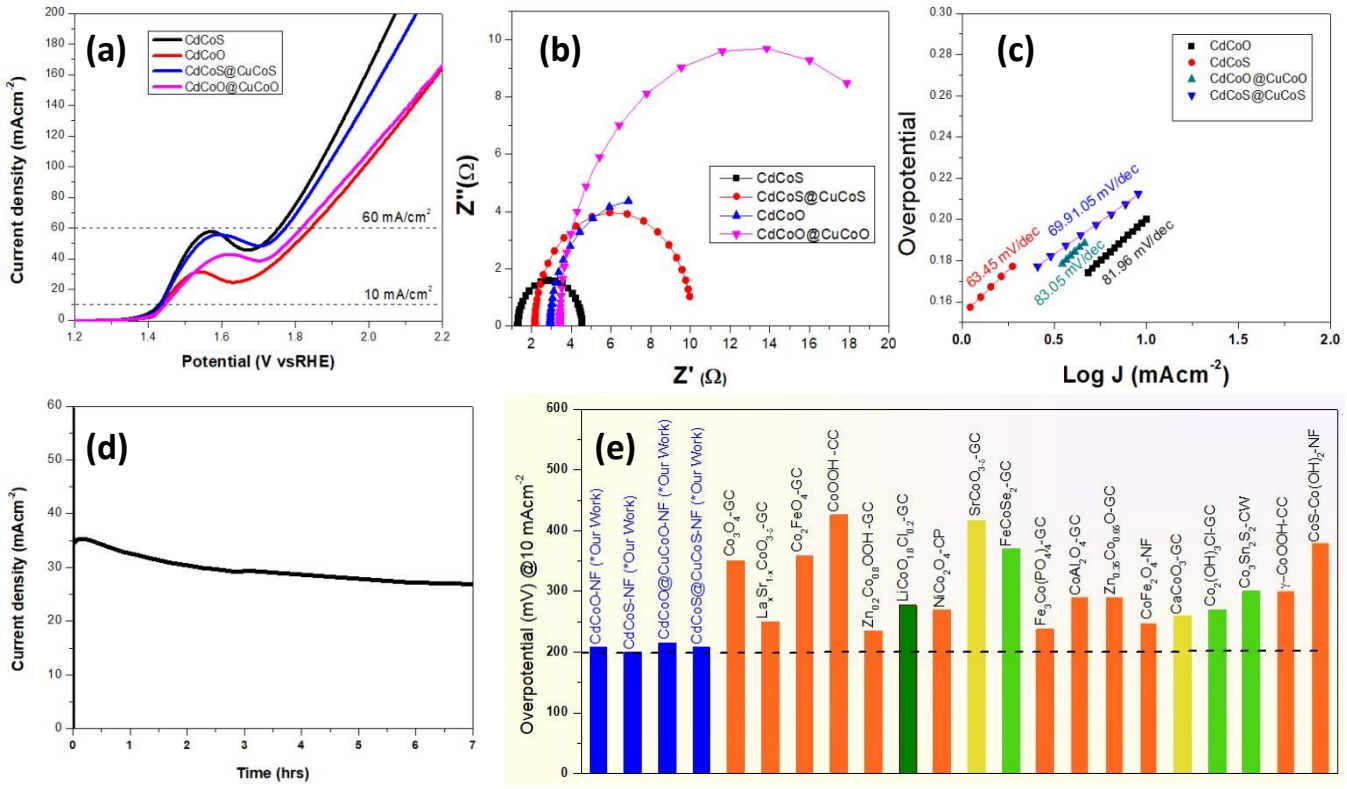

Figure 6. (a) iR uncorrected LSVs (*vs.* RHE), (b) EIS Nyquist plot to determine the charge transfer resistance and solution resistance, (c) Tafel plot to determine the kinetics parameters of as-synthesized CdCoS, CdCoS@CuCoS, CdCoO, and CdCoO@CuCoO. (d) Chronoamperometric stability of the best performing CdCoS electrocatalysts and (e) overpotential at 10 mAcm-2 of the various cobalt-based electrocatalysts for diverse materials class reported in the literature (appropriate references are given in table S1, supporting information); GC = Glassy Carbon, NF = Nickel Foam, CC = Carbon Cloth, CW = Copper Wire, CP = Carbon Paper.

energy for the binding of intermediates can be achieved.[57, 58] Likewise, the sulfides increased the covalency of the M-O bond, and the binding energy of the OER intermediates on the surface of electrocatalysts can be optimized to get improved OER performances.[12] In the present work, the increase in OER activity of CdCoS compared to CdCoO is attributed to the substitution of sulfides.

The incorporation of the Cd in the cobalt oxides/sulfide also influences the electron density of the metal active sites and exposes the active sites by creating defects in the cobalt oxide lattice. The Cd^{2+} has larger ionic radii compared to the Co^{2+}/Co^{3+} ions and has filled 3d orbitals.[59] The large ionic radii produce the distortion in the crystal lattices leading to exposure to the Co-active sites.[18] Moreover, like Zn^{2+},[60] the Cd^{2+} being filled 3d orbitals causes the weak binding with oxygen 2p orbitals leading to localized electron density around the oxygen in the Cd-O bonds. The electronegativity of the Cd^{2+} ions is less than Co^{2+}/Co^{3+} ions thus causing the increase in electron density in the Co^{2+}/Co^{3+} active sites. Thus, excellent OER activity was observed in the CdCoO and CdCoS electrocatalysts compared to various other cobalt oxides(hydroxides), and sulfides of various classes of materials (figure 6e, table S1 supporting information). However, interestingly the OER activity of the electrocatalysts decreased after the formation of the composite. The CdCoO@CuCoO-NCs (CdCoO@CuCoO) were MOF-derived and had two major contributing factors; copper and carbon. The Cu^{2+} ions have a d^9 electronic configuration, have lower electronegativity than $Co^{2+}/Co^{3+,}$ and have similar ionic radii.[59] We propose that the Cu^{2+} incorporation and carbon collectively cover the surface of the materials and remove the surface defects, which we believe collectively lower the catalytic activity of the electrocatalysts. Whereas, the sulfide-based CdCoS@CuCoS electrocatalysts have shown greater OER activity than CdCoO@CuCoO due to the sulfide effect as described above. The OER performance of the CdCoS@CuCoS and CdCoO@CuCoO is still superior to the various reported cobalt-based materials as presented in Figure 6e and Table S1(supporting information).

Conclusions

In summary, the present work reports the intentional designing of multicomponent electrocatalysts by incorporating the Cd in the cobalt oxide to improve oxidative water splitting. The sulfide-modified CdCoS was also synthesized to explore the synergistic effect of Cd incorporation and sulfide effect on the OER performance of electrocatalysts. The CdCoS exhibited the overpotential of 199 mV at 10 $mAcm^{-2}$ which was superior to many of the cobalt-based various materials reported in the literature. The composite of CdCoO and CdCoS was also synthesized with CuCoO and CuCoS via MOF derived route. The resultant CdCoO@CuCoO and CdCoS@CuCoS have exhibited good OER activity, but less than the CdCoO and CdCoS. The lower performance of composites was attributed to the coating of active sites for catalysis. Moreover, the CdCoS also shows good durability after 7 hours of stability testing. This work is expected to provide a venue for the development of efficient electrocatalysts by utilizing a multicomponent doping strategy.

Conflicts of interest

"There are no conflicts to declare".

References

1. T. u. Haq and Y. Haik, in *Electrochemical Water Splitting: Fundamentals, Challenges and Advances*, Springer, 2024, pp. 1-19.
2. M.-I. Jamesh and X. Sun, *Journal of Power Sources*, 2018, **400**, 31-68.
3. K. Li, Y. Tong, J. He, X.-Y. Liu and P. Chen, *Materials Horizons*, 2023, **10**, 5277-5287.
4. H. Wang and H. c. D. Abruña, *The Journal of Physical Chemistry C*, 2021, **125**, 7188-7203.
5. X. Chen, H. Wang, R. Meng, B. Xia and Z. Ma, *ACS Applied Energy Materials*, 2020, **3**, 1305-1310.
6. H. Wang, Y. Tong, K. Li and P. Chen, *Journal of Colloid and Interface Science*, 2022, **628**, 306-314.
7. Y. Tong, P. Chen, L. Chen and X. Cui, *ChemSusChem*, 2021, **14**, 2576-2584.
8. L. Gong, X. Y. E. Chng, Y. Du, S. Xi and B. S. Yeo, *Acs Catalysis*, 2018, **8**, 807-814.
9. X. Cheng and Y. Tong, *ACS Applied Energy Materials*, 2023, **6**, 9577-9584.
10. D. A. Kuznetsov, B. Han, Y. Yu, R. R. Rao, J. Hwang, Y. Román-Leshkov and Y. Shao-Horn, *Joule*, 2018, **2**, 225-244.
11. J. Zheng, D. Meng, J. Guo and Z. Wang, *Journal of Alloys and Compounds*, 2023, **968**, 172254.
12. X. Zhang, H. Zhong, Q. Zhang, Q. Zhang, C. Wu, J. Yu, Y. Ma, H. An, H. Wang and Y. Zou, *Nature Communications*, 2024, **15**, 1383.
13. G. Fu and J.-M. Lee, *Journal of materials chemistry A*, 2019, **7**, 9386-9405.
14. Z. Shao, Q. Zhu, Y. Sun, Y. Zhang, Y. Jiang, S. Deng, W. Zhang, K. Huang and S. Feng, *Advanced Materials*, 2022, **34**, 2110172.
15. J. B. Goodenough and Y. Kim, *Chemistry of materials*, 2010, **22**, 587-603.
16. V. V. Pavlishchuk and A. W. Addison, *Inorganica Chimica Acta*, 2000, **298**, 97-102.
17. A. Padhi, K. Nanjundaswamy, C. Masquelier, S. Okada and J. Goodenough, *Journal of the Electrochemical Society*, 1997, **144**, 1609.
18. H. Yan, R. Deng, S. Zhang, H. Yao, J. Duan, H. Bai, Y. Li, R. Liu, K. Shi and S. Ma, *Journal of Alloys and Compounds*, 2023, **954**, 170072.
19. Q. Zhang, Z. D. Wei, C. Liu, X. Liu, X. Q. Qi, S. G. Chen, W. Ding, Y. Ma, F. Shi and Y. M. Zhou, *International Journal of Hydrogen Energy*, 2012, **37**, 822-830.
20. K. Li and D. Xue, *The Journal of Physical Chemistry A*, 2006, **110**, 11332-11337.
21. K. Li, G. Zhou, Y. Tong, Y. Ye and P. Chen, *ACS Sustainable Chemistry & Engineering*, 2023, **11**, 14186-14196.
22. X. Ren and Y. Tong, *International Journal of Hydrogen Energy*, 2024, **49**, 489-497.

23. K. Li, J. He, X. Guan, Y. Tong, Y. Ye, L. Chen and P. Chen, *Small*, 2023, **19**, 2302130.
24. K. Kannan, D. Radhika, D. Gnanasangeetha, S. K. Lakkaboyana, K. K. Sadasivuni, K. Gurushankar and M. M. J. I. C. C. Hanafiah, 2021, **125**, 108429.
25. A. Q. Mugheri, A. Tahira, U. Aftab, M. I. Abro, A. B. Mallah, G. Z. Memon, H. Khan, M. A. Abbasi, I. A. Halepoto and S. R. J. R. a. Chaudhry, 2019, **9**, 34136-34143.
26. Z. K. Heiba, M. B. Mohamed, M. Abdellatief and A. J. A. P. A. Albassam, 2020, **126**, 1-10.
27. S. Farhadi, M. Javanmard and G. J. A. C. S. Nadri, 2016, **63**, 335-343.
28. V. Revathi and K. J. J. o. M. S. M. i. E. Karthik, 2018, **29**, 18519-18530.
29. K. Kannan, D. Radhika, M. P. Nikolova, V. Andal, K. K. Sadasivuni and L. S. J. O. Krishna, 2020, **218**, 165112.
30. L. Belles, C. Moularas, S. Smykała and Y. J. N. Deligiannakis, 2021, **11**, 925.
31. A. Jena, T. R. Penki, N. Munichandraiah and S. J. J. o. E. C. Shivashankar, 2016, **761**, 21-27.
32. A. M. Mostafa, S. A. Yousef, W. H. Eisa, M. A. Ewaida and E. A. J. A. P. A. Al-Ashkar, 2017, **123**, 1-9.
33. L.-C. Jiang, W.-D. J. B. Zhang and Bioelectronics, 2010, **25**, 1402-1407.
34. L.-L. Ren, L.-H. Wang, Y.-F. Qin and Q. J. F. i. C. Li, 2022, **9**, 818255.
35. S. K. Yadav, A. K. Vishwakarma and L. Yadava, 2023.
36. C. V. Thulasi-Varma, S. S. Rao, C. S. S. P. Kumar, C. V. Gopi, I. K. Durga, S.-K. Kim, D. Punnoose and H.-J. J. D. T. Kim, 2015, **44**, 19330-19343.
37. B. Rivas-Murias and V. J. J. o. R. S. Salgueiriño, 2017, **48**, 837-841.
38. S. Jambure and C. J. M. L. Lokhande, 2013, **106**, 133-136.
39. J. Xu, W. Ji, Z. Shen, W. Li, S. Tang, X. Ye, D. Jia and X. J. J. o. R. s. Xin, 1999, **30**, 413-415.
40. S. Peng, X. Han, L. Li, Z. Zhu, F. Cheng, M. Srinivansan, S. Adams and S. J. S. Ramakrishna, 2016, **12**, 1359-1368.
41. H. Wu and W. J. N. Chen, 2011, **3**, 5096-5102.
42. S. Xie, X. Lu, T. Zhai, J. Gan, W. Li, M. Xu, M. Yu, Y.-M. Zhang and Y. J. L. Tong, 2012, **28**, 10558-10564.
43. Q. Gu, H. Zhuang, J. Long, X. An, H. Lin, H. Lin and X. J. I. J. o. P. Wang, 2012, **2012**.
44. Q. Cheng, C. Yang, K. Tao and L. J. E. A. Han, 2020, **341**, 136042.
45. R. Samal, S. Mondal, A. S. Gangan, B. Chakraborty and C. S. J. P. C. C. P. Rout, 2020, **22**, 7903-7911.
46. T. Mizokawa, Y. Morita, T. Sudayama, K. Takubo, I. Yamada, M. Azuma, M. Takano and Y. Shimakawa, *Physical Review B*, 2009, **80**, 125105.
47. H. Singh, A. Sinha, S. Gupta, M. Singh and H. Ghosh, *arXiv preprint arXiv:1507.05190*, 2015.
48. Y. Ikedo, J. Sugiyama, H. Nozaki, H. Itahara, J. Brewer, E. Ansaldo, G. Morris, D. Andreica and A. Amato, *Physical Review B*, 2007, **75**, 054424.
49. P. Kulkarni, S. Mahamuni, M. Chandrachood, I. Mulla, A. Sinha, A. S. Nigavekar and S. J. J. o. a. p. Kulkarni, 1990, **67**, 3438-3442.
50. K. Gupta, M. Bersani and J. A. J. J. o. M. C. A. Darr, 2016, **4**, 13786-13794.
51. J. Qiao, M. Fan, Y. Fu, Z. Bai, C. Ma, Y. Liu and X.-D. J. E. A. Zhou, 2015, **153**, 559-565.
52. G. Wang, H. Wang, Y. Ling, Y. Tang, X. Yang, R. C. Fitzmorris, C. Wang, J. Z. Zhang and Y. J. N. Li, 2011, **11**, 3026-3033.
53. S. Zhang, D. Li, S. Chen, X. Yang, X. Zhao, Q. Zhao, S. Komarneni and D. J. J. o. M. C. A. Yang, 2017, **5**, 12453-12461.
54. W. Teng, M. Huo, Z. Sun, W. Yang, X. Zheng, C. Ding and S. J. F. i. C. Zhang, 2020, **8**, 334.
55. Y. Song, Y. Guo, S. Qi, K. Zhang, J. Yang, B. Li, J. Chen, Y. Zhao, Y. J. J. o. A. Lou and Compounds, 2021, **884**, 161035.
56. Y. Ning, D. Ma, Y. Shen, F. Wang and X. J. E. A. Zhang, 2018, **265**, 19-31.
57. Z. Wang, Y. You, J. Yuan, Y.-X. Yin, Y.-T. Li, S. Xin and D. Zhang, *ACS applied materials & interfaces*, 2016, **8**, 6520-6528.
58. J. Suntivich, K. J. May, H. A. Gasteiger, J. B. Goodenough and Y. Shao-Horn, *Science*, 2011, **334**, 1383-1385.
59. R. t. Shannon and C. Prewitt, *Acta Crystallographica Section B: Structural Crystallography and Crystal Chemistry*, 1970, **26**, 1046-1048.
60. Z.-F. Huang, J. Song, Y. Du, S. Xi, S. Dou, J. M. V. Nsanzimana, C. Wang, Z. J. Xu and X. Wang, *Nature Energy*, 2019, **4**, 329-338.